

Bond strengthening in lateral heterostructures of transition metal dichalcogenidesIl-Seok Jeong , Eun Gong Ahn, and Joo-Hyoung Lee**School of Materials Science and Engineering, Gwangju Institute of Science and Technology, Gwangju, Republic of Korea*

(Received 31 December 2019; revised 6 August 2020; accepted 10 August 2020; published 25 August 2020)

The adhesion strength of lateral heterostructures composed of transition metal dichalcogenides (MoS_2 , MoSe_2 , WS_2 , and WSe_2) monolayers is investigated with first-principles electronic structure calculations. Our density functional theory calculations demonstrate that the adhesion strength, which is gauged by the ideal work of separation (W_{sep}), strongly depends on the local atomic configuration, and that W_{sep} becomes enhanced (diminished) at the interface where a chalcogen atom forms bonds with one (two) W and two (one) Mo atoms compared to those of the homogeneous cases. It is further shown that the increase (decrease) in W_{sep} from the homogeneous value is caused by the charge redistribution among the interfacial bonds, which is determined by the differences in the electronegativity of the transition metal species at the interface. Such geometrically controlled interfacial strength presents a route to control the materials' mechanical characteristics through structural engineering.

DOI: [10.1103/PhysRevB.102.075441](https://doi.org/10.1103/PhysRevB.102.075441)**I. INTRODUCTION**

Two-dimensional (2D) monolayer (ML) materials have received considerable attention due to their novel physical properties that are not typically observed in their three-dimensional counterparts [1]. Among various 2D ML materials, transition metal dichalcogenides (TMDCs) in the form of MX_2 , where M and X are transition metal species and chalcogen atoms, respectively, have been the subject of a multitude of studies. The particular interest in TMDCs stems from their distinctive material characteristics such as high carrier mobility [2] and direct band gap [3,4], which are especially appealing for photonic and optoelectronic applications.

Besides the compelling electronic properties, the mechanical properties of ML TMDCs have also been extensively investigated both experimentally and theoretically [5–12]. First-principles studies on the mechanical properties of TMDCs reported that the elastic moduli of MoX_2 are 223 (S), 179 (Se), and 126 (Te) GPa under uniaxial strain, respectively. The dependence of elastic modulus on the transition metal species is due to the charge reorganization taking place during the formation of a compound from individual atoms [11]. On the experimental side, measurements on the mechanical properties of ML MoS_2 with an atomic force microscope discovered that the average elastic modulus and breaking strength are 180 ± 60 and $15 \pm 3 \text{ N m}^{-1}$, respectively [12]. While these values are not as high as those of graphene, which is known as the most reliable 2D material [13], they are still sufficiently large to make ML TMDCs ultrastrong materials capable of withstanding substantial external strain.

Meanwhile, the structural similarity between dissimilar TMDCs allows one to investigate more complex ML structures such as composites of two different TMDCs. Indeed,

recent advances in synthetic technology have made it possible to form in-plane heterostructures where different types of TMDC MLs are laterally stitched with sharp atomic-level one-dimensional boundaries [14–24]. Such planar heterostructuring provides an opportunity to realize unique characteristics which are lacking in the homogeneous MLs. For instance, lateral heterojunctions formed with MoSe_2 and WSe_2 exhibit enhanced photoluminescence [14], p - n diodes and photodiodes are produced in WS_2/WSe_2 lateral heterojunctions [15], and a p - n junction is formed within ML WSe_2 - MoS_2 systems [17]. Moreover, theoretical studies have shown that electronic structures such as band gaps, band alignment, and charge transport can be tuned by adjusting the width of each TMDC region [25–28]. All these findings surely signify the potential of TMDC lateral heterostructures as atomically thin systems integrated with device functionalities.

Contrary to numerous studies on the electronic and optoelectronic properties of ML TMDC heterostructures, however, their mechanical properties have received less attention [29]. When two homogeneous materials are combined to form interfaces, the adhesion strength among others is of special importance from the stability's point of view because heterointerfaces are generally considered weaker than homogeneous materials under external strain. In examining the adhesion strength, the ideal work of separation (W_{sep}), which is defined as the reversible work to separate the interface into two free surfaces [30], plays a key role as a quantitative metric. Since a higher W_{sep} implies more energy required to rupture a material, the ideal work of separation has been constantly employed to analyze the adhesion properties of various metal/ceramic and metal/metal interfaces to design novel compounds with enhanced performance [31–35].

In this paper, we carry out first-principles density functional theory (DFT) calculations to calculate W_{sep} of in-plane ML TMDC heterostructures and investigate the mechanical strength of the interfaces. By considering the heterostructures

*jhyoung@gist.ac.kr

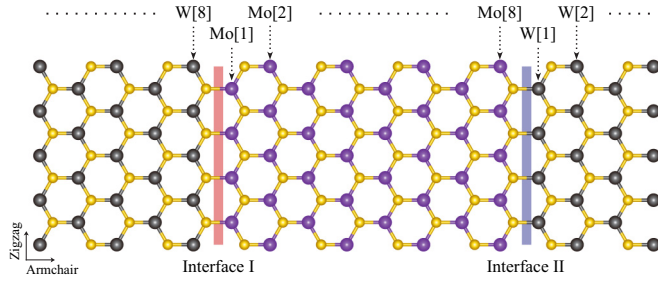


FIG. 1. Geometry of a $[\text{MoX}_2]_4[\text{WX}_2]_4$ lateral heterostructure ($X = \text{S, Se}$) with Mo, W, and X illustrated with purple, gray, and yellow spheres, respectively. The interfaces I and II are highlighted in red and blue, respectively.

which are composed of molybdenum (MoX_2) and tungsten dichalcogenides (WX_2) with $X = \text{S}$ and Se , it is demonstrated that W_{sep} of the heterointerfaces can be higher than those of homogeneous ML MX_2 . Since such a variation in W_{sep} is further shown to depend on the local atomic environment at the interface, our results suggest a route toward tuning the mechanical properties through interface engineering [36–41].

II. COMPUTATIONAL DETAILS

All first-principles calculations are conducted within DFT with the frozen-core projector augmented method [42] as implemented with the Vienna *ab initio* simulation package [43,44]. The Kohn-Sham wave functions are expanded in terms of the plane-wave basis with a 600 eV cutoff, and a generalized gradient approximation is employed to treat the exchange-correlation energy between electrons [45]. All atomic positions are optimized until the Hellmann-Feynman force acting on each atom becomes less than 0.05 eV/Å. For the Brillouin zone integration, $13 \times 3 \times 1$ and $25 \times 7 \times 1$ \mathbf{k} -point meshes are employed in cases of structural optimization and W_{sep} calculations, respectively. Also, to avoid spurious interactions between adjacent layers arising from a periodic boundary condition, a 15 Å vacuum region is included perpendicular to the layers.

The computational geometry of the TMDC heterostructures employed in the present study is illustrated in Fig. 1. As is seen from the figure, the supercell consists of four MoX_2 and four WX_2 units along the armchair direction, denoted as $[\text{MoX}_2]_4[\text{WX}_2]_4$ hereafter, because the zigzag-type interfaces have been reported as the most favorable heterostructures in experiment [19,27]. It should be noted that since the mismatch in lattice constants (a) is small between MoX_2 and WX_2 ($\sim 4.2\%$) as is shown in Table I, it is thus allowed to take into account only a coherent interface model for the heterostructures.

To calculate the ideal work of separation, an external strain (ε) is applied in the armchair direction of the $[\text{MoX}_2]_4[\text{WX}_2]_4$ heterostructure through increasing the corresponding lattice constant by a finite amount (δ). The strained structure is then fully relaxed, and the entire cycle (strain followed by relaxation) is sequentially repeated by gradually increasing δ . At each $\varepsilon = \delta/L_0$ with L_0 the unstrained lattice constant, we compute the strain energy as $E_s(\varepsilon) = E(\varepsilon) - E_0$, where

TABLE I. Lattice constant (a), ideal work of separation (W_{sep}), and charge difference ($\Delta Q_{[M]}$) of MX_2 monolayers. The numbers in the parentheses are the fraction with respect to the initial charge $Q_{[M]}$.

	a (Å)	W_{sep} (eV)	$\Delta Q_{[M]}$ (e)
MoS_2	3.19	4.47	-1.16 (-9.7%)
MoSe_2	3.19	4.10	-0.90 (-7.5%)
WS_2	3.33	4.83	-1.31 (-10.9%)
WSe_2	3.33	4.14	-1.00 (-8.3%)

$E(\varepsilon)$ and E_0 are the total energies of the fully relaxed systems with and without the strain, respectively. When the system is strained, $E_s(\varepsilon)$ increases quadratically with ε and reaches a maximum at a critical value (ε^*). Once ε exceeds ε^* , the heterostructure ruptures and $E_s(\varepsilon)$ abruptly decreases to a constant value, which is W_{sep} .

As will be shown below, however, the above approach only leads to breaking the weakest bond in the heterostructure. Since it is our purpose to compare the strengths of the different bonds, we also compute W_{sep} for each M - X bond along the armchair direction. To this end, a large separation (l) is introduced into one of the M - X bonds, and the ideal work of separation is obtained with $W_{\text{sep}} = E_l - E_0$, with E_l and E_0 being the total energies of separated and unseparated systems, respectively. For complete cleavage of the bonds, $l = 20$ Å is employed in calculations.

III. RESULTS AND DISCUSSION

Before delving into the ideal work of separation for various cases, it should be noted that $n = 4$ in $[\text{MoX}_2]_n[\text{WX}_2]_n$ is found to be sufficient in producing well-converged W_{sep} within less than 2 meV compared to higher n values. We first inspect W_{sep} of homogeneous ML MX_2 , which is listed in Table I. As is seen from the table, W_{sep} of WX_2 is higher than that of the corresponding MoX_2 , and sulfides have a larger W_{sep} than selenides. To understand this tendency, we employ the Bader charge analysis [46,47] and define the charge difference ($\Delta Q_{[M]}$) as

$$\Delta Q_{[M]} = Q_{[\text{MX}_2]} - Q_{[M]}. \quad (1)$$

Here, $Q_{[\text{MX}_2]}$ and $Q_{[M]}$ are the Bader charge around a transition metal element in a MX_2 structure and as an isolated atom, respectively. Apparently, there is a charge transfer from a transition metal to a chalcogen element [11], which is revealed by the negative $\Delta Q_{[M]}$ in Table I. Notably, $|\Delta Q_{[M]}|$ is the largest for WS_2 (10.9%) and smallest for MoSe_2 (7.5%), respectively. This is because (i) S has a higher electronegativity than Se and (ii) there are more s electrons in W than in Mo. It should be noted that the variation in $\Delta Q_{[M]}$ is in the same order as W_{sep} , which is due to the enhanced covalency between M and X atoms (thus a stronger M - X bonding) contributed by high $|\Delta Q_{[M]}|$ values.

Let us examine the adhesion behavior of the lateral heterostructures. In Fig. 2(a), the ratio of the M - X bond lengths of $[\text{MoS}_2]_4[\text{WS}_2]_4$ heterostructures is presented in the cases of four different strain values. Here, the ratio (R_d) is defined as $R_d = [d_{M-X}(\varepsilon) - d_{M-X}]/d_{M-X}$, where $d_{M-X}(\varepsilon)$ and d_{M-X} are the M - X bond lengths with and without external strain,

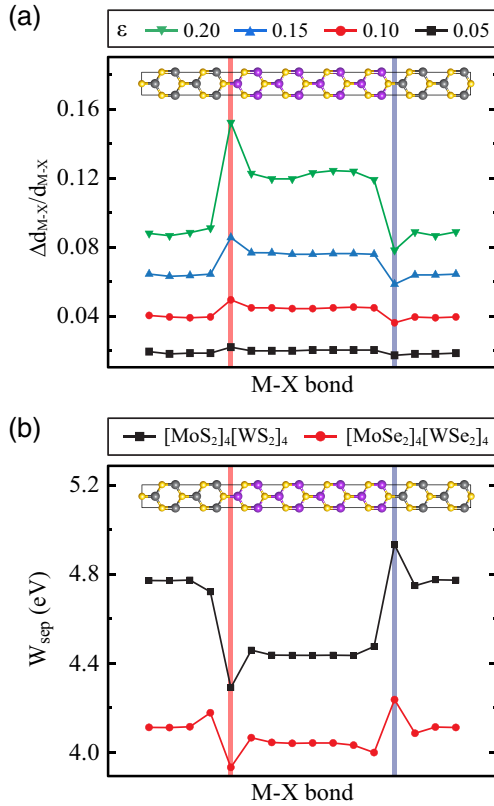


FIG. 2. (a) The ratio of the M - X bond lengths in the $[\text{MoS}_2]_4[\text{WS}_2]_4$ heterostructure between the strained and unstrained cases, and (b) W_{sep} at each of the M - X bonds. $\Delta d_{M-X} = d_{M-X}(\epsilon) - d_{M-X}$, and red and blue vertical regions represent interface I and II, respectively.

respectively. When weakly strained ($\epsilon < 0.05$), all bonds are equally stretched regardless of the transition metal species as is seen from nearly equal R_d values: $R_d = 0.019$ and 0.018 in the MoS₂ and WS₂ regions, respectively. As the strain rises further, however, the molybdenum and tungsten regions are differently stretched in that R_d of MoS₂ increases more rapidly than that of WS₂. While R_d grows from 0.038 to 0.084 for WS₂ as the strain becomes enhanced from 0.1 to 0.2, the corresponding values change from 0.043 to 0.115 for MoS₂, which indicates that WS₂ is stiffer and mechanically stronger than MoS₂ as is manifested by the higher W_{sep} values (Table I). It should be noted that R_d of the selenides shows the same tendency as the sulfides.

Interestingly, the interfacial bonds between MoS₂ and WS₂ exhibit highly unique responses to strain, which differ from the interior regions. At interface I, where a sulfur atom is neighbored with two W and one Mo atoms (Fig. 1), the Mo-S bond is stretched more easily than the ones away from the interface. The interfacial bond is prolonged by 9.3% more than the Mo-S bonds within the MoS₂ region for $\epsilon = 0.1$, and the extension becomes even more pronounced at higher strain in that the bond is elongated by 24.1% more under 20% of strain. However, when two Mo and one W atoms form bonds with the S atom (interface II in Fig. 1), the W-S bond is less stretched than the bonds inside the WS₂ region. At each strain

value ($\epsilon = 0.1, 0.15$, and 0.2), the W-S bond at interface II is elongated by 3.7, 6.0, and 8.2%, respectively, whereas the corresponding stretches of the interior W-S bonds are 3.8, 6.1, and 8.4%, respectively.

The opposite behavior of the interfacial bonds against external strain suggests that interface I and II be mechanically weaker and stronger than the interior TMDC regions, respectively. Indeed, when strained further, the Mo-S bond at interface I of $[\text{MoS}_2]_4[\text{WS}_2]_4$ eventually ruptures at $\epsilon^* = 0.212$, resulting in $W_{sep} = 4.30$ eV. Similar calculations with the selenide heterostructure reveal that $\epsilon^* = 0.236$ and $W_{sep} = 3.94$ eV, respectively.

To gain an insight into the adhesion strength, the ideal work of separation is calculated for each of the M - X bonds in the heterostructures and presented in Fig. 2(b). As is seen from the figure, the average values of W_{sep} are 4.45 and 4.05 eV for the bonds' interior MoS₂ and MoSe₂ regions, and 4.77 and 4.13 eV for the WS₂ and WSe₂ cases, respectively. It should be noted that these values are almost the same as those of homogeneous ML monolayers (Table I), which implies that the mechanical strength of the M - X bonds distant from the interfaces remains essentially unaffected. Compared to the above results, W_{sep} of the MoS(e)₂ region is higher than that of the $[\text{MoS(e)}_2]_4[\text{WS(e)}_2]_4$ heterostructure by 155 (110) meV, confirming that interface I makes the weakest bond. However, it should be noted that the highest W_{sep} occurs at interface II for both S (4.94 eV) and Se (4.25 eV) cases, which together with the smallest elongation of the bond demonstrates that this type of interface will become even stronger than the homogeneous cases against strain.

To understand the origin of the contrasting behavior in the adhesion strength at the two interfaces, especially the bond strengthening at interface II, we present in Fig. 3 the projected density of states (PDOS) onto each atom in the $[\text{MoS}_2]_4[\text{WS}_2]_4$ heterostructure. As is seen from Figs. 3(a) and 3(b), PDOS of the transition metal elements of the interior MX_2 region are almost the same as that of the homogeneous MLs. However, the PDOS of M at the interfaces displays a noticeable difference: While remaining close to that of the interior for $-4.0 \text{ eV} \lesssim E \leq 0 \text{ eV}$, the PDOS of Mo and W at the interfaces shifts in energy downward and upward for $E < -4.0 \text{ eV}$, respectively, compared to the interior cases. For the Mo cases, the peaks in the interfacial PDOS for $E < -4.0 \text{ eV}$ are downshifted by 0.22 and 0.11 eV and they are upshifted by 0.24 and 0.14 eV for the W cases, respectively. As a result of the shifts, the PDOS of the interfacial Mo and W agrees well with each other as is seen from Figs. 3(c) and 3(d). Interestingly, such a concurrence is mediated by the chalcogen atom between Mo and W, which is evidenced by the resonance peaks in the PDOS of the S p orbitals below $E = -4.0 \text{ eV}$. It should be noted that $[\text{MoSe}_2]_4[\text{WSe}_2]_4$ also shows similar shifts in the PDOS.

The aforementioned hybridization of the electronic states has a significant impact on the bond strength at the interfaces. To analyze the effect of the PDOS restructuring on the bond strength, we compute the bond order (BO) for each bond in the heterostructures. To this end, we employ an atomic population analysis method, the density derived electrostatic and chemical approach (DDEC6), which is based on a dressed exchange

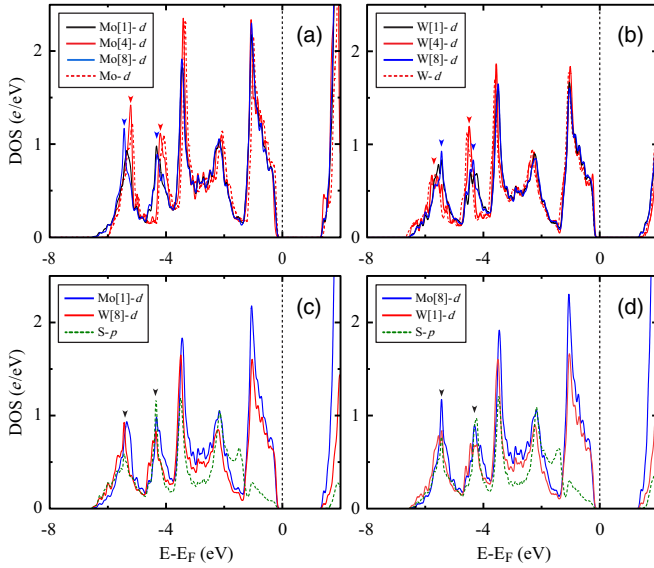


FIG. 3. The PDOS of (a) Mo and (b) W in $[\text{MoS}_2]_4[\text{WS}_2]_4$. The black, red, and blue solid lines represent the d orbital of Mo (W) at interface I (II), the interior region, and interface II (I), respectively. The red dotted lines are for the homogeneous MLs. The PDOS of Mo d and W d orbitals at interface I and II are displayed in (c) and (d), respectively, together with that of S p orbitals, which is depicted in green. E_F denotes the Fermi energy, and arrows indicate the peaks in the PDOS.

hole partitioned among atoms and provides satisfactory results for a wide variety of materials [48,49].

Figures 4(a) and 4(b) show the computed BO for W-X and Mo-X bonds in the interior regions of $[\text{MoX}_2]_4[\text{WX}_2]_4$, respectively. As is presented in Figs. 4(a) and 4(b), all three bonds from the chalcogen atom have the same BO values. We find that these values differ from the homogeneous MLs

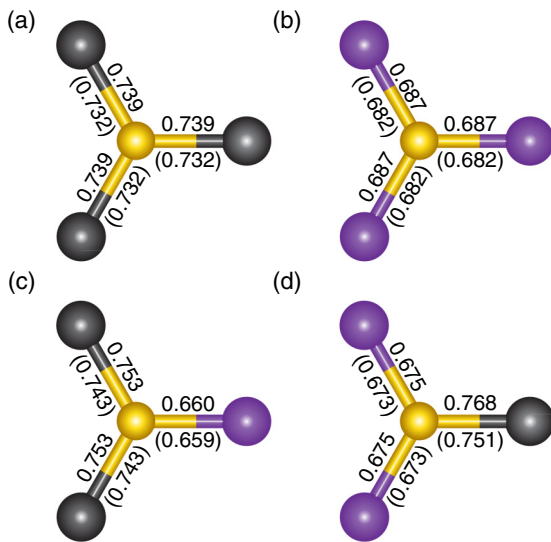


FIG. 4. Bond order of (a) WS_2 and (b) MoS_2 in their interior regions of the heterostructure. (c) and (d) represent the BO at interface I and II, respectively. In all cases, the numbers in the parentheses are for selenides.

by at most 0.7%, which again evidences that the mechanical strength of the interior regions would be the same as that of the homogeneous cases. It is worth noting that WS_2 has a higher BO than MoS_2 and that the BO of the sulfides is greater than that of the selenides. Recalling that the BO essentially measures the number of electrons participating in the bond, the bond between W (Mo) and S (Se) will be the strongest (weakest) among the MLs, which is in accord with W_{sep} in Table I.

In Figs. 4(c) and 4(d) we present the BOs at interface I and II, respectively. As is clear from the figures, the threefold symmetry that is present in the interior BOs is broken at the interfaces. For both interfaces, the BO between Mo and X is reduced from the interior values, whereas it is enhanced for the W-X bonds. Specifically, at interface I the BOs of Mo-S and Mo-Se decrease by 3.9% and 3.4%, and they increase by 1.9% and 1.5% for W-S and W-Se, respectively. On the other hand, the reduction in the BOs of Mo-S and Mo-Se is 1.8% and 1.3%, and the enhancement for W-S and W-Se is 3.9% and 2.6% at interface II, respectively. Such a reorganization in the BO leads to the twofold symmetry with respect to the horizontal M -X bond.

It is interesting to observe that the total reduced BO in the Mo-X bonds is nearly equal to the total BO gain in the W-X bonds. Since the BO is proportional to the number of electrons, the resulting variation in the interfacial BOs indicates that electrons are transferred from Mo-X bonds to W-X bonds and thus the corresponding bonds weaken and strengthen, respectively. We note that the electron transfer arises from the difference in the electronegativity (χ) of the transition metal elements. Since χ of Mo and W is 2.16 and 2.36, respectively, in the Pauling scale, the electrons at the Mo-X bonds are attracted toward the W-X bonds and thus the depletion and accumulation of electrons is induced at the interfaces.

IV. SUMMARY

In summary, we have studied the mechanical strength of in-plane TMDC heterostructures by calculating the ideal work of separation with first-principles DFT calculations. It is demonstrated that, except for the interfaces, the ideal work of separation of the heterostructure is close to that of the homogeneous monolayers. This suggests that the mechanical strength is well preserved within the interior of each TMDC region.

On the other hand, the interfaces display quite different behavior from the interior under strain, which depends on the local atomic environment. In particular, it is the number of Mo and W atoms forming bonds with an interfacial chalcogen atom that leads to the difference in the mechanical strength. In homogeneous cases, each chalcogen atom makes bonds with three M elements, all of which are the same kind. At the interfaces, however, one M is different from the others, and the difference in the electronegativity of the transition metal elements brings about asymmetric distribution in the bond order, which results from the electron transfer from Mo-X to W-X bonds. In more realistic situations, an interface would contain both types of interfaces considered here (interface I and II) and line shapes (zigzag or armchair). Even in such cases, the adhesion strength can be estimated by taking into

account the relative fraction of the different transition metal species connected with chalcogen atoms.

Finally, we note that the electronegativity-induced electron transfer mechanism is not limited to the TMDC heterostructures as in the present study. Through sophisticated structural engineering of the atomic configuration at the interfaces, the mechanical behavior can be regulated via a similar mechanism.

ACKNOWLEDGMENT

This research has been performed as a cooperation project of “Basic Project (referring to projects performed with the budget directly contributed by the Korean Government to achieve the purposes of establishment of Government-funded Research Institutes)” and supported by the Korea Research Institute of Chemical Technology (KRICT, SI 2051-10).

-
- [1] A. K. Geim, *Science* **324**, 1530 (2009).
- [2] B. Radisavljevic, A. Radenovic, J. Brivio, V. Giacometti, and A. Kis, *Nat. Nanotechnol.* **6**, 147 (2011).
- [3] H. Ramakrishna Matte, A. Gomathi, A. K. Manna, D. J. Late, R. Datta, S. K. Pati, and C. Rao, *Angew. Chem., Int. Ed.* **49**, 4059 (2010).
- [4] A. Ramasubramaniam, *Phys. Rev. B* **86**, 115409 (2012).
- [5] T. Li, *Phys. Rev. B* **85**, 235407 (2012).
- [6] R. C. Cooper, C. Lee, C. A. Marianetti, X. Wei, J. Hone, and J. W. Kysar, *Phys. Rev. B* **87**, 035423 (2013).
- [7] C. Ataca, H. Sahin, and S. Ciraci, *J. Phys. Chem. C* **116**, 8983 (2012).
- [8] K. Liu, Q. Yan, M. Chen, W. Fan, Y. Sun, J. Suh, D. Fu, S. Lee, J. Zhou, S. Tongay *et al.*, *Nano Lett.* **14**, 5097 (2014).
- [9] D. Çakır, F. M. Peeters, and C. Sevik, *Appl. Phys. Lett.* **104**, 203110 (2014).
- [10] J. Kang, H. Sahin, and F. M. Peeters, *Phys. Chem. Chem. Phys.* **17**, 27742 (2015).
- [11] J. Li, N. V. Medhekar, and V. B. Shenoy, *J. Phys. Chem. C* **117**, 15842 (2013).
- [12] S. Bertolazzi, J. Brivio, and A. Kis, *ACS Nano* **5**, 9703 (2011).
- [13] C. Lee, X. Wei, J. W. Kysar, and J. Hone, *Science* **321**, 385 (2008).
- [14] C. Huang, S. Wu, A. M. Sanchez, J. J. Peters, R. Beanland, J. S. Ross, P. Rivera, W. Yao, D. H. Cobden, and X. Xu, *Nat. Mater.* **13**, 1096 (2014).
- [15] X. Duan, C. Wang, J. C. Shaw, R. Cheng, Y. Chen, H. Li, X. Wu, Y. Tang, Q. Zhang, A. Pan, J. Jiang, R. Yu, Y. Huang, and X. Duan, *Nat. Nanotechnol.* **9**, 1024 (2014).
- [16] Y. Gong, J. Lin, X. Wang, G. Shi, S. Lei, Z. Lin, X. Zou, G. Ye, R. Vajtai, B. I. Yakobson *et al.*, *Nat. Mater.* **13**, 1135 (2014).
- [17] M.-Y. Li, Y. Shi, C.-C. Cheng, L.-S. Lu, Y.-C. Lin, H.-L. Tang, M.-L. Tsai, C.-W. Chu, K.-H. Wei, J.-H. He *et al.*, *Science* **349**, 524 (2015).
- [18] Y. Gong, S. Lei, G. Ye, B. Li, Y. He, K. Keyshar, X. Zhang, Q. Wang, J. Lou, Z. Liu *et al.*, *Nano Lett.* **15**, 6135 (2015).
- [19] X.-Q. Zhang, C.-H. Lin, Y.-W. Tseng, K.-H. Huang, and Y.-H. Lee, *Nano Lett.* **15**, 410 (2014).
- [20] K. Bogaert, S. Liu, J. Chesin, D. Titow, S. Gradečak, and S. Garaj, *Nano Lett.* **16**, 5129 (2016).
- [21] J. Chen, W. Zhou, W. Tang, B. Tian, X. Zhao, H. Xu, Y. Liu, D. Geng, S. J. R. Tan, W. Fu *et al.*, *Chem. Mater.* **28**, 7194 (2016).
- [22] K. S. Novoselov, A. Mishchenko, A. Carvalho, and A. H. Castro Neto, *Science* **353**, aac9439 (2016).
- [23] M.-Y. Li, J. Pu, J.-K. Huang, Y. Miyauchi, K. Matsuda, T. Takenobu, and L.-J. Li, *Adv. Funct. Mater.* **28**, 1706860 (2018).
- [24] S. Xie, L. Tu, Y. Han, L. Huang, K. Kang, K. U. Lao, P. Poddar, C. Park, D. A. Muller, R. A. DiStasio, and J. Park, *Science* **359**, 1131 (2018).
- [25] M. Aras, Ç. Kılıç, and S. Ciraci, *J. Phys. Chem. C* **122**, 1547 (2018).
- [26] H. Jin, V. Michaud-Rioux, Z.-R. Gong, L. Wan, Y. Wei, and H. Guo, *J. Mater. Chem. C* **7**, 3837 (2019).
- [27] Y. Guo and J. Robertson, *Appl. Phys. Lett.* **108**, 233104 (2016).
- [28] V. Mishra and S. Salahuddin, *IEEE Trans. Nanotechnol.* **17**, 1053 (2018).
- [29] Y.-J. Zhang, R.-N. Wang, G.-Y. Dong, S.-F. Wang, G.-S. Fu, and J.-L. Wang, *AIP Adv.* **9**, 125208 (2019).
- [30] M. W. Finnis, *J. Phys.: Condens. Matter.* **8**, 5811 (1996).
- [31] J.-H. Lee, T. Shishidou, Y.-J. Zhao, A. J. Freeman, and G. B. Olson, *Philos. Mag.* **85**, 3683 (2005).
- [32] D. F. Johnson, D. Jiang, and E. A. Carter, *Surf. Sci.* **601**, 699 (2007).
- [33] D. F. Johnson and E. A. Carter, *J. Phys. Chem. A* **113**, 4367 (2009).
- [34] D. H. R. Fors and G. Wahnström, *Phys. Rev. B* **82**, 195410 (2010).
- [35] T. E. Jones, M. E. Eberhart, S. Imlay, C. Mackey, and G. B. Olson, *Phys. Rev. Lett.* **109**, 125506 (2012).
- [36] T. Georgiou, R. Jalil, B. D. Belle, L. Britnell, R. V. Gorbachev, S. V. Morozov, Y.-J. Kim, A. Gholinia, S. J. Haigh, O. Makarovsky *et al.*, *Nat. Nanotechnol.* **8**, 100 (2013).
- [37] Z. Liu, L. Ma, G. Shi, W. Zhou, Y. Gong, S. Lei, X. Yang, J. Zhang, J. Yu, K. P. Hackenberg *et al.*, *Nat. Nanotechnol.* **8**, 119 (2013).
- [38] K. Chen, X. Wan, J. Wen, W. Xie, Z. Kang, X. Zeng, H. Chen, and J.-B. Xu, *ACS Nano* **9**, 9868 (2015).
- [39] W. Wei, Y. Dai, and B. Huang, *Phys. Chem. Chem. Phys.* **19**, 663 (2017).
- [40] J. Lee, J. Huang, B. G. Sumpter, and M. Yoon, *2D Mater.* **4**, 021016 (2017).
- [41] C. Zhang, M.-Y. Li, J. Tersoff, Y. Han, Y. Su, L.-J. Li, D. A. Muller, and C.-K. Shih, *Nat. Nanotechnol.* **13**, 152 (2018).
- [42] P. E. Blöchl, *Phys. Rev. B* **50**, 17953 (1994).
- [43] G. Kresse and J. Hafner, *Phys. Rev. B* **47**, 558 (1993).
- [44] G. Kresse and J. Furthmüller, *Phys. Rev. B* **54**, 11169 (1996).
- [45] J. P. Perdew, K. Burke, and M. Ernzerhof, *Phys. Rev. Lett.* **77**, 3865 (1996).
- [46] R. F. W. Bader, P. L. A. Popelier, and T. A. Keith, *Angew. Chem. Int. Ed.* **33**, 620 (1994).
- [47] W. Tang, E. Sanville, and G. Henkelman, *J. Phys.: Condens. Matter* **21**, 084204 (2009).
- [48] T. A. Manz and N. G. Limas, *RSC Adv.* **6**, 47771 (2016).
- [49] T. A. Manz, *RSC Adv.* **7**, 45552 (2017).